Spin dephasing of electrons and holes in isotopically purified ZnSe/(Zn,Mg)Se quantum wells

N. E. Kopteva ●,[1,2] E. Kirstein,[2] E. A. Zhukov,[2,3] M. Hussain,[4] A. S. Bhatti,[4] A. Pawlis,[5] D. R. Yakovlev,[2,3]
M. Bayer,[2,3] and A. Greilich[2]

[1]*Spin Optics Laboratory, St. Petersburg State University, Ul'anovskaya 1, Peterhof, St. Petersburg 198504, Russia*
[2]*Experimentelle Physik 2, Technische Universität Dortmund, 44221 Dortmund, Germany*
[3]*Ioffe Institute, Russian Academy of Sciences, 194021 St. Petersburg, Russia*
[4]*Center for Micro and Nano Devices (CMND), Department of Physics, COMSATS University Islamabad, Park Road,
Islamabad 44000, Pakistan*
[5]*Peter Grünberg Institute (PGI-9), Forschungszentrum Jülich, 52425 Jülich, Germany*

The coherent spin dynamics of resident electrons and holes in an isotopically purified ZnSe/(Zn,Mg)Se single quantum well is investigated in different regimes, requiring corresponding adaption of the applied time-resolved pump-probe Kerr rotation technique. The purification of the Zn and Se atom species in the crystal to the isotopes with zero nuclear spin is expected to lead to an extension of the spin dephasing times of resident carriers, due to the suppression of their interaction with the nuclear spins. Indeed, we find no indication of carrier-nuclear interaction in this sample and link the observed carrier spin relaxation to the spin-orbit interaction. Theoretical considerations support the experimental results.

I. INTRODUCTION

Several mechanisms of spin relaxation of resident charge carriers in semiconductor heterostructures are related to the spin-orbit interaction requiring motion of the carriers during which they undergo scattering [1,2]. In low-dimensional heterostructures motion becomes suppressed; for example, in quantum wells (QWs) the carriers are strongly confined along the growth direction, but are in an ideal structure free to move in the well plane. However, in real structures, resident carriers can be also hindered in their in-plane motion due to localization in QW width fluctuations, depending on temperature and carrier density. These fluctuations result from monolayer steps at the heterointerfaces formed during molecular-beam epitaxy (MBE) growth. While spin-orbit related relaxation is suppressed thereby, localized carriers have increased interaction with the surrounding nuclear spins of the constituting crystal material. This interaction leads to spin relaxation related to fluctuations of the nuclear fields [1].

The influences of localization and nuclei on the carrier spin relaxation were previously studied in different types of QW structures, which include the material combinations GaAs/(Al,Ga)As [3,4], CdTe/(Cd,Mg)Te [5–8], and ZnSe/(Zn,Mg)Se [8,9]. Particular attention in these studies was devoted to measuring the spin dephasing and relaxation times as important indicators of the spin coherence in a carrier ensemble.

As indicated, for strongly localized carriers in small magnetic fields, the spin dephasing time is limited by the interaction with the fluctuating surrounding of nuclear spins. There are several ways to circumvent this limitation: (i) decreasing the nuclear field fluctuations, or (ii) reducing the carrier interaction with nuclei. To have a significant effect, the first strategy requires almost complete polarization of the nuclei

along one direction; so far no experimental evidence for such high polarization has been reported [10]. The second strategy can be pursued by using isotopically purified materials. Purification is especially favorable in II-VI materials, which typically have small nuclear spins and even isotopes with zero nuclear spins. In particular, for the ZnSe material system with isotopic purification by ^{64}Zn and ^{80}Se with zero nuclear spin, it should be possible to eliminate the nuclear effect on the carrier spin dephasing and uncover further mechanisms responsible for spin dephasing.

In this paper, we study the spin dynamics of resident electrons and holes in an isotopically purified ZnSe/(Zn,Mg)Se QW structure. Time-resolved pump-probe Kerr rotation is used to measure the time evolution of the optically induced spin coherence for different experimental conditions. The effects of excitation power, additional illumination, temperature, and magnetic field on the spin-relaxation properties are considered. Ultimately, we conclude that the spin-orbit interaction is the primary reason for the observed spin relaxation.

II. EXPERIMENTAL DETAILS

The studied ZnSe/Zn$_{0.85}$Mg$_{0.15}$Se QW heterostructure was grown in an MBE machine equipped with specially designed Knutsen evaporation cells filled with isotopically purified Zn and Se [11]. The cells allow for fast temperature ramping and stabilization within 30 min. The sample was grown on a (100)-oriented GaAs substrate followed by an 8-nm-thick ZnSe buffer layer to obtain a smooth and abrupt interface between III-V and II-VI materials. The structure contains a 16-nm ZnSe single QW surrounded by 25-nm-thick Zn$_{0.85}$Mg$_{0.15}$Se barriers. We estimated the isotope purification grade of the material in our MBE chamber by secondary ion mass spectrometry (SIMS) on a series of reference samples (for details

see Ref. [11]). From the SIMS data, we quantified the isotope purity of the as-grown structure for the zero spin isotopes ^{64}Zn and ^{80}Se to be 99.985% and 99.997%, respectively, within the QW, the barriers, and the buffer. The $Zn_{0.85}Mg_{0.15}Se$ barrier contains in addition magnesium (^{25}Mg) having 10% natural abundance of an isotope with nuclear spin $I = 5/2$. Even if the sample is nominally undoped, the measured signals indicate a low density of resident electrons and holes at low temperatures. These carriers are expected to arise from MBE chamber residuals. Namely, we estimate an n-type background carrier concentration in the order of 1×10^{16} cm^{-3} from residual fluorine atoms, which act as donor centers when a fluorine replaces a selenium atom [12].

The sample is placed in a vector magnet system consisting of three superconducting split coils oriented orthogonal to each other. It allows us to switch the magnetic field from the Faraday geometry (magnetic field $B_{\parallel}$ is parallel to the light wave vector coinciding with the sample growth axis) to the Voigt geometry (magnetic field $B_{\perp}$ is perpendicular to the light wave vector) without changing the position of the laser beam on the sample. The maximum field along the three directions is 3 T. The measurements are performed in a temperature range from $T = 1.8$ up to 60 K.

The pump-probe time-resolved degenerate Kerr rotation (TRKR) technique [13,14] is used to study the dynamics of electron and hole spins in magnetic fields of various orientations. The pulse emission from a mode-locked Ti:sapphire laser (pulse duration of 1.5 ps and a repetition period $T_R = 13.2$ ns) is frequency doubled using a beta-barium borate crystal, which allows tuning of the photon energy in the range 2.801–2.810 eV, and then is divided into the pump and probe beams. The polarization of the pump is modulated between σ^+ and σ^- either by a photoelastic modulator at 50 kHz or by an electro-optical modulator (EOM) with variable modulation frequency in the range of $f_m = 0.002$–25 MHz. The EOM version of the setup allows us to study the spin-relaxation time using the spin-inertia method [15–17].

The pump-induced spin coherence is detected in reflection geometry by Kerr rotation (KR) of the linearly polarized probe using a balanced photoreceiver with lock-in detection. The pump beam has a 350-μm spot size on the sample; the spot diameter of the probe beam is slightly smaller. The probe power is 0.5 mW and the pump power is varied in the range 1.5–10 mW. The spin dynamics are also measured with additional above-barrier illumination by a continuous-wave (cw) laser with photon energy of 3.06 eV at different power.

The TRKR can be adapted such that three different spin dynamics regimes can be addressed: (i) The KR angle is measured in dependence on the delay time between pump and probe pulses in transverse magnetic field $B_{\perp}$. This signal shows damped periodic oscillations, from which the carrier g factors and their spin-relaxation times can be extracted in the limit $T_2^* < T_R$. (ii) In resonant spin amplification (RSA) [14,18], the KR signal has not yet decayed and a finite nonzero polarization is left at the moment of next pump pulse arrival, if $T_2^* > T_R$. The dependence of the KR signal amplitude on the transverse magnetic field at small negative delays (-50 ps) shows periodic peaks. The separation between the peaks gives the carriers' g factors. The peak width is determined by the spin-relaxation time, and the decrease in peak amplitude with
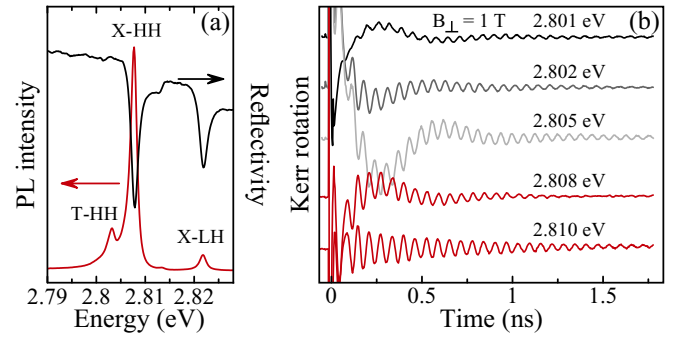

FIG. 1. (a) The red line is the photoluminescence spectrum of the studied sample for nonresonant excitation at 3.06 eV. The black line is the reflectivity spectrum. (b) TRKR signal at different energies of excitation. $T = 1.8$ K, $B_{\perp} = 1$ T, and $P_{\text{pump}} = 3$ mW.

increasing magnetic field is caused by the spread of g factors. (iii) To obtain polarization recovery curves (PRCs) [13], the amplitude of the KR signal is measured at a fixed negative delay time (-50 ps) as for RSA, but in dependence on a longitudinal magnetic field $B_{\parallel}$. In weak fields, the carriers lose their initial polarization due to interaction with residual effective magnetic fields. As the field rises further, the carrier spins stabilize and the average spin polarization increases. As a result, the PRC curve has a dip around zero magnetic field. The width of this dip allows one to directly measure the effective fields. By varying the f_m of the EOM, one also gets access to the spin lifetime T_s of carriers for $T_s > T_R$.

The photoluminescence (PL) spectrum is measured using a cw laser with photon energy of 3.06 eV for excitation. The reflection spectrum is measured using a halogen lamp. The spectra are recorded by a Peltier-cooled charge-coupled device camera (PIXIS: 400B) attached to a 0.5 m spectrometer.

III. EXPERIMENTAL RESULTS

A. KR regime

Figure 1(a) shows the PL and reflectivity spectra of the studied sample. The observed spectral lines correspond to the excitons consisting of an electron and a heavy hole (X-HH) at 2.8073 eV or a light hole (X-LH) at 2.8213 eV. In addition, the less intense line of the heavy-hole trion (T-HH) consisting of two electrons paired to a singlet state and a heavy hole is visible at 2.8027 eV in the PL spectrum.

Next, KR is measured by tuning the wavelength of the pump pulses in the energy range corresponding to the heavy-hole trion and exciton. Figure 1(b) shows KR signals measured for different laser excitation energies $\hbar\omega = 2.801$–2.810 eV in a transverse external magnetic field $B_{\perp} = 1$ T. All traces show fast and slow oscillations which can be related to the Larmor precession of the electron and hole spins, respectively [9]. The amplitude ratio of these two components varies with the excitation energy. In the region of high energies the fast oscillating signal dominates, while at the low-energy side the fast oscillations are practically absent.
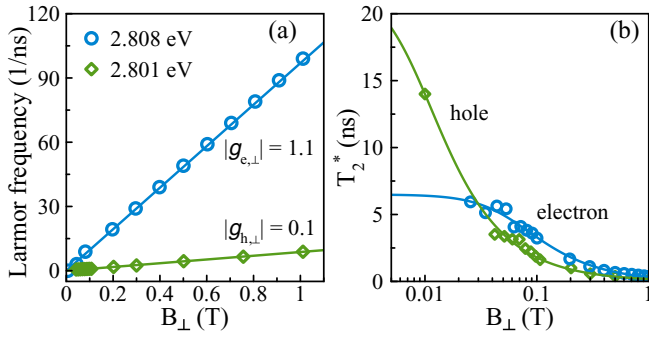
FIG. 2. (a) Dependence of Larmor frequencies on magnetic field for the hole component (green diamonds) measured at 2.801 eV and the electron component (blue circles) measured at 2.808 eV. Lines are fits with $\omega_{e(h)} = \mu_B g_{e(h)} B_\perp/\hbar$. (b) Spin dephasing time dependence on magnetic field. The green and blue lines are fits to the data using Eq. (2). $T = 1.8$ K, $P_{pump} = 1.5$ mW.

For a detailed analysis of the experimental data the KR signal is fitted using the form

$$S(t) = \sum_{i=e,h} A_i \cos(\omega_i t) \exp\left(-\frac{t}{T_{2,i}^*}\right), \qquad (1)$$

where $S(t)$ is the z component of the spin polarization, and $A_{e(h)}$ and $T_{2,e(h)}^*$ are the amplitudes and spin dephasing times of the resident electron and hole contributions, respectively. $\omega_{e(h)} = g_{e(h)} \mu_B B_\perp/\hbar$ are the Larmor frequencies of resident electron and hole spin precession in the external magnetic field $B_\perp$, and μ_B is the Bohr magneton. g_e and g_h are the in-plane g factors of electron and hole, respectively. t is the delay time between the pump and probe pulses.

Figure 2(a) shows the Larmor frequency dependence on the external magnetic field with linear-in-B fits, whose slopes are determined by the g factors of the resident electrons, $|g_e| = 1.10 \pm 0.01$, and holes, $|g_h| = 0.10 \pm 0.01$. The magnetic field dependencies of the spin dephasing times for electrons measured at 2.808 eV and for holes measured at 2.801 eV are shown in Fig. 2(b). These dependencies are well described by the following equation [12]:

$$T_{2,e(h)}^* = \hbar/\sqrt{(\Delta g_{e(h)} \mu_B B_\perp)^2 + (g_{e(h),\perp} \mu_B \Delta B_{e(h)})^2}. \qquad (2)$$

In high magnetic fields the spin dephasing time decreases with growing $B_\perp$ and is limited by the spread of the carrier g factors $\Delta g_{e(h)}$. In the range of small magnetic fields, the second term in Eq. (2) dominates. Here the $\Delta B_{e(h)}$ represents residual effective magnetic fields responsible for the spin dephasing. In isotopically nonpurified structures, these are usually ascribed to the fluctuating nuclear fields, which act on the carrier spins through the hyperfine interaction [1,12].

A fit to the data with function of Eq. (2) gives the following parameters: $\Delta g_e = 0.03$ for the spread of electron g factor, which is about 2% of the absolute g factor; $\Delta g_h = 0.06$ for the spread of hole g factors, about 67% of absolute g factor [19]; and $\Delta B_e = 1.6$ mT and $\Delta B_h = 5.1$ mT, characterizing the limiting factors at low magnetic fields. Accordingly, the T_2^* of electrons and holes at low fields reach the maximal values of 7 and 19 ns, respectively, for the used pump power.

TABLE I. Comparison of isotopically purified (ISO) sample of this paper, and nonpurified (non-ISO) sample of $ZnSe/Zn_{0.89}Mg_{0.11}S_{0.18}Se_{0.82}$ QW (sample 3 from Ref. [9]).

	$T_{2,e}^*$	$T_{2,h}^*$	$g_{e,\parallel}$	$g_{e,\perp}$	Δg_e	$g_{h,\parallel}$	$g_{h,\perp}$	Δg_h
ISO	7 ns	19 ns	1.15	1.11	0.03	1.0	0.1	0.06
non-ISO	20 ns	0.8 ns	1.18	1.13		1.8	0.06	0.03

Note that the electron dephasing time at zero magnetic field in the isotopically purified QW is about three times shorter than the previously reported $T_{2,e}^* = 20$ ns for nonpurified ZnSe/(Zn,Mg)(S,Se) QWs [9]. For a simplified comparison, parameters for both types of samples are collected in Table I.

Attention should also be driven to the significantly longer hole spin dephasing time which is by more than an order of magnitude higher than the previously reported one [9] of $T_{2,h}^* = 0.8$ ns. Further, the spread of hole g factor is slightly increased (previously published [9] $|g_h| = 0.06$ and $\Delta g_h = 0.03$).

It is known that the nominal heavy-hole state gains its finite g factor in the QW plane due to mixing of light hole and heavy hole [9]. This mixing is determined by the structural parameters of the QW [20]. In Fig. 3 we show measurements of the g factors in the $\perp$ - $\parallel$ plane for both carriers, namely, as a function of the angle ψ between the field direction and an in-plane direction. The following equation was used for fitting the data:

$$g_{\perp,\parallel} = \sqrt{g_{e(h),\perp}^2 \cos^2(\psi) + g_{e(h),\parallel}^2 \sin^2(\psi)}. \qquad (3)$$

The fitting gives $|g_{h,\parallel}| = 1.00 \pm 0.01$ for the holes and $|g_{e,\parallel}| = 1.15 \pm 0.01$ for the electrons, which is in good comparison with the values in Ref. [21].

To obtain more insight into the mechanisms responsible for spin relaxation, we also measured the temperature dependence of the spin dephasing times (see Fig. 4). The data were extracted from KR signals in a transverse magnetic field of $B_\perp = 0.5$ T. The inspection of the dependencies shows that the behavior for both types of carriers is similar. The dephasing times are constant up to $T = 20$ K and are limited by the g-factor spreads. At higher temperatures ($T > 20$ K)
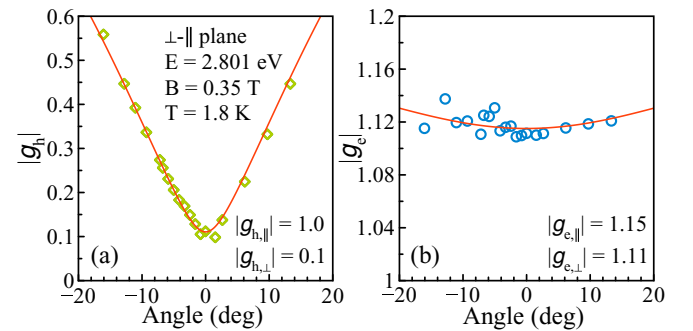

FIG. 3. (a) Dependence of g factor on the angle between the field and an in-plane direction of the QW for the hole (a) and electron (b), measured at 2.801 eV. The lines are fits to the data using Eq. (3). $P_{pump} = 2$ mW.
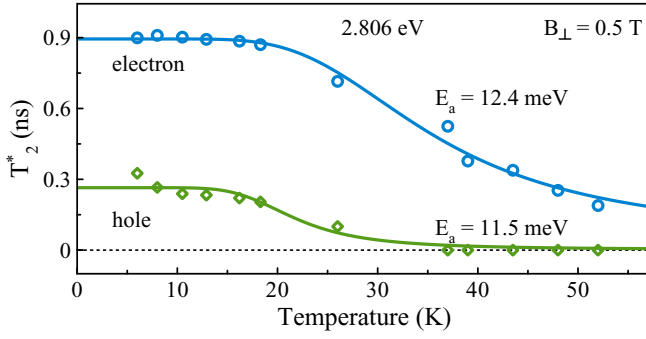
FIG. 4. Temperature dependence of spin dephasing times of electrons and holes. Symbols are experimental data and lines are fits with Eq. (4) using the following parameters: $T_0^e = 0.89$ ns, $T_0^h = 0.26$ ns, $T_{exc}^e = 18.7$ ps, $T_{exc}^h = 0.6$ ps, $E_a^e = 12.4$ meV, $E_a^h = 11.5$ meV. $\hbar\omega = 2.806$ eV, $P_{pump} = 2.5$ mW.

the dependencies drop due to delocalization of the carriers so that the spin-relaxation mechanisms become related to free movement of the carriers in the QW plane [1].

The measured dependencies can be fitted by an Arrhenius-type equation, which describes the thermal activation from a localized ground state with long relaxation time $T_0^{e(h)}$ to an excited state with a shorter relaxation time $T_{exc}^{e(h)}$:

$$\frac{1}{T_{2,e(h)}^*} = \frac{1}{T_0^{e(h)}} + \frac{1}{T_{exc}^{e(h)}} \exp\left(-\frac{E_a^{e(h)}}{k_B T}\right). \quad (4)$$

Here $E_a^{e(h)}$ is the activation energy of the localized carriers and k_B is the Boltzmann constant. Fitting gives for electrons and holes $E_a^e = 12.4$ meV and $E_a^h = 11.5$ meV, respectively.

The obtained activation energies are, on the one hand, smaller than the fluorine-bound electron activation energy of 29.3 ± 0.6 meV measured for an epilayer structure [12,22]. On the other hand, they are quite large for potentials arising from fluctuations of the QW composition or thickness. As noted in the Ref. [23], a low-magnesium mole fraction should reduce the alloy fluctuations in the ternary material in both barrier and QW. In our sample, the magnesium concentration is significant, about 15%. Therefore, we can assume that there are significant fluctuations in the QW thickness, which could lead to the significant modifications of the electron and hole localization potentials.

B. RSA studies (transverse magnetic field)

Additional information on the electron and hole spin dynamics can be obtained from analyzing RSA curves. The resident carrier spins precess about the external magnetic field with their Larmor frequencies $\omega_{e(h)}$ determined by their g factors and the field $B_\perp$. If the precession frequency equals an integer number of the laser repetition frequency ($\omega_R = 2\pi/T_R$) and the spin coherence time is at least comparable with T_R, spin polarization will be accumulated, and the dependence of KR on magnetic field shows periodic peaks at integer values of the ratio $\omega_{e(h)}/\omega_R$.

Figure 5(a) shows RSA traces measured for different excitation energies. All RSA signals contain two components centered around zero magnetic field. The first RSA component
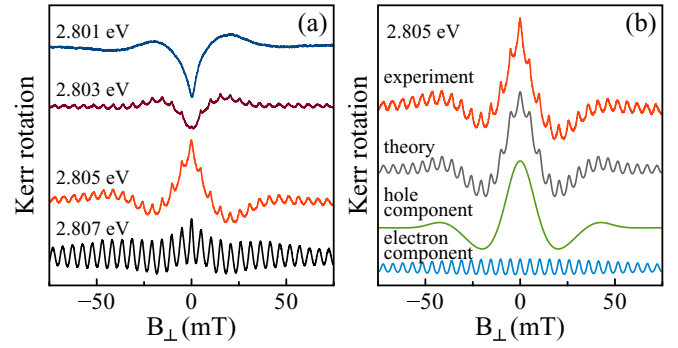

FIG. 5. (a) Experimental RSA traces for different excitation energies. (b) Measured RSA in comparison to calculated RSA signal, as well as the decomposition into electron and hole contributions (shifted for clarity) to the RSA signal at 2.805 eV. $P_{pump} = 1.5$ mW.

is a set of equidistant peaks with a period of about 5 mT, and an amplitude, which gradually decreases with an increasing magnetic field. This component is associated with the Larmor precession of electron spins around the external magnetic field. The second component is due to the precession of the hole spins: the presence of only one strong peak (around zero field) in this case indicates a small g-factor value and a significant spread of g factors.

To estimate the parameters of the spin-relaxation times, $g_{e(h)}$ factors, spreads $\Delta g_{e(h)}$, and amplitudes of the electron and hole contributions, the RSA is calculated according to the approach described in Refs. [18,24]. The RSA curve is given by the following equation:

$$S_{e(h)}^- = \frac{\Theta^2}{16} \frac{\exp(-T_R/T_{2,e(h)}) - \cos(\omega_{e(h)}T_R)}{\cosh(T_R/T_{2,e(h)}) - \cos(\omega_{e(h)}T_R)}. \quad (5)$$

Here $T_{2,e(h)}$ is the spin coherence time of a resident electron or hole. Equation (5) is a simplified form of Eq. (29) in Ref. [24] for resonant optical excitation and $\Theta = 0.1\pi$ pulse area. As mentioned above, the g-factor spreads for electrons and holes are [18,25]

$$\rho(g_{e(h)}) = \frac{1}{\sqrt{2\pi}\Delta g_{e(h)}} \exp\left[\frac{-(g_{e(h)} - g_{0,e(h)})^2}{2(\Delta g_{e(h)})^2}\right]. \quad (6)$$

$g_{0,e(h)}$ are the average g-factor values in the spin ensemble, corresponding to average Larmor frequencies. To be more specific, we calculate $S_{e(h)}^-$ for each $g_{e(h)}$ factor within the spreads $\Delta g_{e(h)}$ and numerically integrated over $\Delta g_{e(h)}$. The final RSA curve is the sum of integrated S_e^- and S_h^-. As an example, the measured RSA for 2.805 eV is compared to the calculated RSA signal in Fig. 5(b), together with the separate electron and home components.

The comparison gives the following results: $|g_h| = 0.10$ and $\Delta g_h = 0.06$. These values coincide well with the values obtained from fitting of the KR signals. This, in its turn, confirms the earlier assumption about a significant dispersion of the hole localization potentials in our sample. As a result, the RSA signal for the hole component has only one peak centered at zero magnetic field [see Fig. 5(a)] [19].

The amplitude ratio of the two RSA components varies with the excitation energy. Changes in this ratio show a similar character for the RSA signal and for the KR signal. As will be
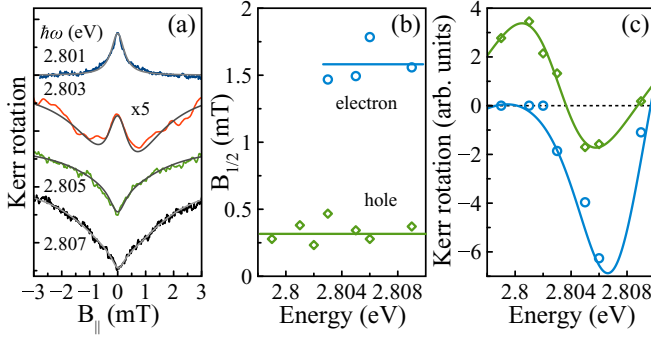
FIG. 6. (a) Experimental PRC signals for different excitation energies. The black lines are fits to the data using Eq. (7). (b) Dependence of the HWHM of PRC signals on excitation energy. (c) Amplitude dependence of electron and hole contribution to PRC on excitation energy. Lines are guides to the eyes. $T = 1.8$ K and $P_{\mathrm{pump}} = 1.5$ mW.

FIG. 7. Spin inertia curves at 2.801 eV (a) and 2.806 eV (b) for $B_\parallel = 7$ mT, $T = 1.8$ K, and $P_{\mathrm{pump}} = 2.7$ mW.

shown below, this ratio also changes with additional above-barrier illumination and excitation power.

C. PRC studies (longitudinal magnetic field)

Now we discuss the results of the PRC technique, described in Sec. II. Figure 6(a) shows PRC curves measured for different excitation energies, where we observe a two-peak structure: the narrow peak exists across the full range of energies and represents the hole spins, while the wide peak only appears for energies above 2.803 eV, and is ascribed to the electrons. This behavior of the electron component in the PRCs is in good agreement with its appearance in RSA curves, as shown in Fig. 5(a). The features of the PRC shapes in Fig. 6 also correlate well with the features of the KR and RSA signals: in the low-energy range, the hole component dominates the signal.

For analysis, we use fits to the data by either one or two Lorentz curves having the form

$$ S_z = \frac{S_0 B_\parallel^2}{B_\parallel^2 + B_{1/2}^2}. \tag{7} $$

S_0 is the initial electron (hole) polarization, and $B_{1/2}$ is the half width at half maximum (HWHM) of the peak (or the dip). The dependencies of $B_{1/2}$ and S_0 on excitation energy are shown in Figs. 6(b) and 6(c). The HWHM of both components is constant across the entire range of the energies, while the amplitudes vary strongly, demonstrating a dominant hole contribution at the lower energy side, while the electron component dominates at the higher flank.

Next, we present the results of spin-inertia measurements and determine the spin-relaxation time T_s [15]. An increase of the modulation frequency f_m of the EOM leads to a decrease of the spin-polarization degree when $f_m \gg T_s^{-1}$. In the experiment the lock-in amplifier records the following signal:

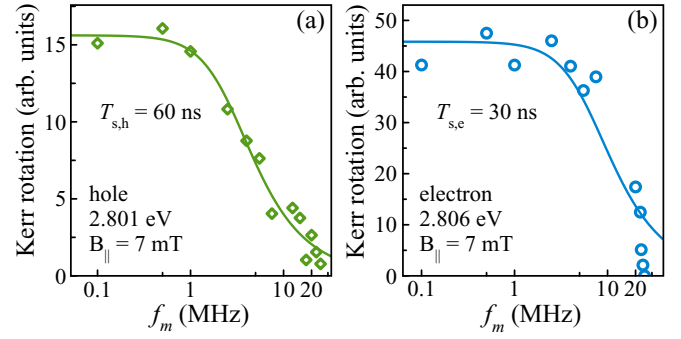$$ |L(f_m)| = \frac{2}{\pi} \frac{n_0 |S_0|}{\sqrt{1 + (2\pi f_m T_s)^2}}. \tag{8} $$

n_0 is the resident electron (hole) concentration, $|S_0|$ is the initial carrier spin polarization, $1/T_s = 1/\tau + 1/\tau_s$, τ is the lifetime of the photogenerated carriers, and τ_s is the spin-relaxation time at zero excitation power.

Figures 7(a) and 7(b) show the dependencies of the PRC amplitudes at fixed longitudinal magnetic field ($B_\parallel = 7$ mT) on modulation frequency measured at 2.801 and 2.806 eV, respectively. These dependencies can be fitted by Eq. (8), leading to $T_{s,h} = 60$ ns at 2.801 eV and $T_{s,e} = 30$ ns at 2.806 eV. The spin-relaxation time of electrons is not as long as for electrons strongly localized at fluorine donors (400 ns), as reported in Ref. [15]. It allows us to conclude that the smaller localization energy of carriers trapped on QW fluctuation potentials is decisive for their spin lifetime. As a consequence, T_s limits the spin coherence time for the electron (hole) in an ensemble ($T_2 \leqslant 2T_s$). Usually, one has to perform a series of T_s measurements at different pump powers, to extract the intrinsic spin-relaxation time (τ_s) by extrapolation to zero power. However, the strong dependence of the relative carrier fractions on the excitation power (see below) does not allow us to determine this time accurately for both components [15].

D. Effects of above-barrier illumination and pump power

Let us first analyze the situation with additional above-barrier illumination. We demonstrate the effect of illumination at photon energy of 2.806 eV, as here the pumping controls the concentration of resident carriers and thereby changes the ratio of the electron and hole components. Fitting of the experimentally measured RSA curves at various illumination intensities shows the following results (Fig. 8): (i) The amplitude of the hole component decreases sharply to almost zero with the increase of illumination power [Fig. 8(c)]. In parallel, the amplitude of the electron component remains nearly constant for the additional illumination intensities used in the experiment. We conclude that the above-barrier illumination shifts the balance of resident carriers in favor of the electrons. (ii) The dephasing time of the electron spins increases approximately 1.5-fold and reaches a constant value of 11 ns, while the hole spin dephasing time decreases by more than a factor of 4 from 12 ns down to 3 ns, which is apparently due to the compensation of holes by photoexcited electrons [Fig. 8(b)]. Similar changes in the ratio of the electron and hole components in the signal of ZnSe-based quantum wells
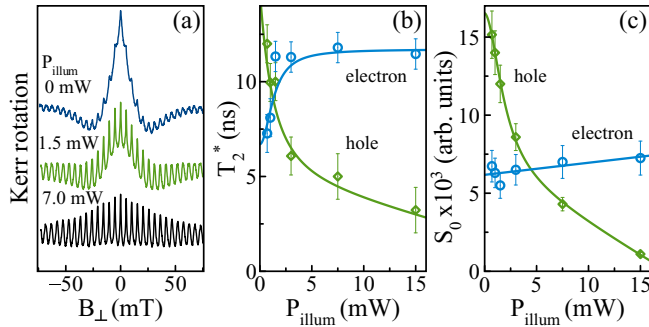
FIG. 8. (a) Above-barrier illumination (3.06 eV) intensity dependence of RSA signal for 2.806 eV at $T = 1.8$ K. (b) Dephasing time dependence on illumination power for the electron (blue circles) and hole (green diamonds) components. (c) Dependence of the electron and hole component amplitudes on illumination intensity. $P_{pump} = 1$ mW. Lines are guides to the eyes.

FIG. 10. PRC (green line) and RSA (blue line) traces at energies of 2.801 eV (a) and 2.807 eV (b).

(not isotopically purified) were observed and discussed in Ref. [9].

As noted earlier, an increase of the pump pulse intensity leads to the appearance and growth of the electron component and a decrease of the hole component in the KR signal. Similar to the case with additional illumination, we use the RSA to analyze the dynamics of carriers [Fig. 9(a)]. Figure 9(b) shows the spin-relaxation time of the electron and hole spin components vs pump power. The observed dependencies demonstrate that the hole T_2^* drops threefold with increasing pump power; simultaneously the electron T_2^* weakly increases. A similar effect is observed in experiments with additional above-barrier illumination. Figure 9(c) shows the spin amplitude as a function of pump power. The amplitude of the electron component saturates with increasing pump power, while the amplitude of the hole spin component increases first and then decreases for pump powers higher than 4 mW, which is apparently due to the hole compensation process by photoexcited electrons.

IV. DISCUSSION

Before we turn our attention to the mechanisms responsible for carrier relaxation, let us recollect the magnetic field dependencies for the electron and hole RSA and PRC signals in Fig. 10. It is interesting to compare the widths of the zero-field RSA peaks and PRC dips measured at the same energies in two spectral ranges: (a) when the hole component dominates the signal, and (b) when the electron component dominates.

Figure 10(b) does that for the electron component; both dependencies have a similar peak width. This is the usual case for electrons with an isotropic *g* factor that the zero RSA and PRC peaks have comparable widths. The holes, in contrast, demonstrate quite a strong difference of the widths [Fig. 10(a)]. This can be related to the strong anisotropy of the hole *g* factor; in our case by a factor of 10. Additionally, the PRC peak width is determined by the effective magnetic field created by the fluctuating nuclei. If nuclear interaction is present, the PRC peak width for the holes should be much narrower than for the electron. This is related to the very weak hole-nuclear coupling, about one order of magnitude weaker than for electrons [26–29].

Nanostructures grown with materials isotopically purified towards zero nuclear spins attract attention primarily by the fact that the carrier spins do not interact with the nuclear spins. In particular, this should lead to a suppression of spin relaxation by nuclear spin fluctuations [30,31]. Therefore, a significant increase of the spin-relaxation time in small magnetic fields and an absence of polarization recovery effects (i.e., the PRC dip should be absent) are expected. However, as shown by our measurements (Fig. 10), this expected behavior is not observed. The following mechanisms may lead to a limitation of the spin-relaxation times in our sample [32]: (i) the Bir-Aronov-Pikus mechanism, (ii) spin relaxation caused by nuclear spin fluctuations, (iii) spin-orbit relaxation caused by exchange-induced spin diffusion.

The main reason for spin relaxation in the Bir-Aronov-Pikus mechanism (i) is the exchange scattering of electrons on holes. This process is significant only for spin dynamics of carriers bound to an exciton. Therefore, it should not affect the spin relaxation of resident carriers tested here.

Process (ii) is possible for nuclei with nonzero spins. There are four types of nuclei in the structure under study: ^{80}Se and
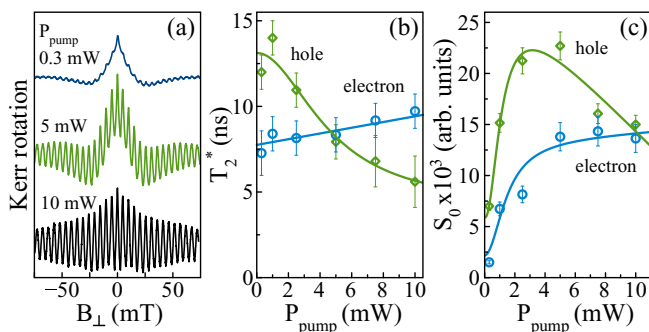

FIG. 9. (a) Pump power dependence of RSA for excitation energy 2.806 eV at $T = 1.8$ K. (b) Dephasing time dependencies on pump power for the electron (blue circles) and hole (green diamonds) components. (c) Dependence of electron and hole component amplitudes on pump power. Lines are guides to the eyes.
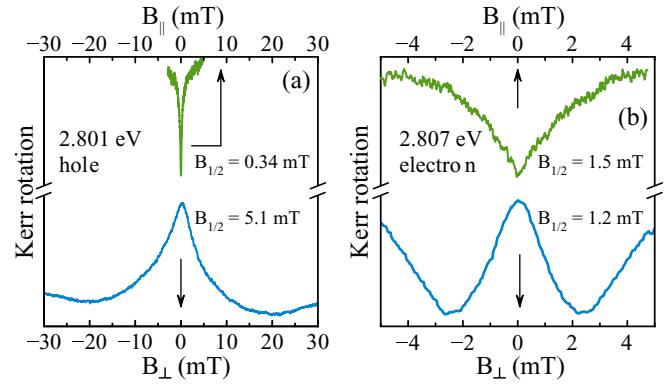
[64]Zn with zero spin, [25]Mg with $I = 5/2$ in the QW barriers with 10% abundance, and [19]F ($I = 1/2$, 100% abundance) at a concentration of 1×10^{16} cm^{-3} due to a background doping. We performed thorough tests to detect traces of nuclear polarization: (a) the system showed no response corresponding to the nuclear magnetic resonance of Zn or Se in the RSA signal at different frequencies of polarization modulation and powers of excitation; (b) the RSA peaks are not shifting with an increasing pump power [33]. It should be noted that control measurements on ZnSe/(Zn,Mg)Se QWs grown from conventional, nonpurified materials show positive results for both tests, i.e., they demonstrate the presence of nuclear spins [34,35].

Next, we consider the depolarizing effect of the residual nuclear spins of fluorine on the longitudinal electron spin polarization. If any fluctuating nuclear fields are present, these are going to reduce the electron spin polarization at weak magnetic fields [31]. Once the external longitudinal magnetic field $B_\parallel$ with strength comparable to the nuclear fields is applied, it stabilizes the carrier spin polarization (see Eq. (7)) [30,31]. First, we want to estimate the effective magnetic field produced by the residual fluctuating fluorine nuclei. The maximal effective nuclear field (Overhauser field) produced by fully polarized nuclei at the electron positions can be estimated as [36]

$$B_{N,max} = \frac{A_{hf}\chi I_F}{g_e\mu_B},$$ (9)

with $A_{hf} = 200$ μeV is the fluorine hyperfine constant [12] and $I_F = 1/2$ is the fluorine spin. The fluorine abundance $\chi = n_F/n$, with $n_F = 1 \times 10^{16}$ cm^{-3} being the approximate fluorine concentration, and n is the concentration of atoms in a ZnSe unit cell. Calculating the volume of the unit cell V_0 with eight atoms from the lattice constant 0.566 nm, $n = 8/V_0 = 4.42 \times 10^{22}$ cm^{-3}. This leads to an effective fluorine abundance of $\chi = n_F/n = 2.3 \times 10^{-7}$.

Estimation of the Overhauser field with these parameters gives $B_{N,max} = 0.37$ μT. The fluctuating field can be described by the Gaussian statistics, which leads to $B_f = B_{N,max}/\sqrt{N}$, with N being the number of nuclei in the localization volume of a fluorine bounded electron. Taking the upper limit with $N = 1$ and $B_f = 0.37$ μT, the spin lifetime time caused by this field can be estimated as $T_s = T_2^* = \hbar/(g_e\mu_B B_f) = 175$ μs for the electron component with $g_e = 1.1$. As one can see, this time is four orders of magnitude longer than the one seen in the experiment.

Furthermore, one can estimate [37] that the probability of penetration of the electron and hole wave functions localized in the QW into the barrier is less than 1% due to a high effective mass ($m_e = 0.146m_0$ and $m_h = 0.96m_0$) and the large barrier height ($V_e = 57.6$ meV and $V_h = 13.4$ meV) [23]. Therefore, carriers should not interact with the Mg isotopes in the barriers efficiently enough, that the relaxation observed in the experiment could be explained.

We finally consider the relaxation process (iii) based on the spin-orbit interaction. In Ref. [2] several mechanisms of spin-relaxation acceleration due to spin-orbit interaction for electrons localized on donors were proposed. It was concluded that the mechanism of exchange spin-orbit interaction is the most effective for donor-localized electron spins, once the spin relaxation on nuclear spin fluctuations is not taken into account. Additionally to the exchange interaction, the hopping of the carriers between the occupied localization potentials and the unoccupied ones can be considered as an effective magnetic field, which accelerates the spin relaxation. The hopping and exchange interaction mechanisms depend on the overlap of the wave functions of electrons localized on two donors. However, the realization of the hopping mechanism requires the presence of unoccupied donors and is strongly suppressed at a low temperatures, as the jumps occur with the photon emission or absorption [2]. In what follows, we neglect the hopping and only consider the exchange spin-orbit interaction.

The next equation allows one to calculate the spin-orbit interaction constant for an electron in the conduction band of a crystal with zinc-blende structure, as expressed in Eq. (3.2a) of Chapter 3 in Ref. [32]:

$$\alpha_{SO} = \frac{2\gamma_c}{\hbar^3}\sqrt{2m_e^3 E_g}.$$ (10)

$\gamma_c = 1.62$ eV Å^3 is the coefficient of the spin splitting of the Γ_6 conduction band [38]. $E_g = 2.82$ eV is the band-gap energy. This leads to $\alpha_{SO}(\text{ZnSe}) = 0.021$ [5].

Further, we estimate the spin-relaxation time and the effective magnetic field caused by the spin-orbit exchange interaction. The spin part of the wave functions for localized electrons depends on the distance from the donor. Therefore, the wave functions for electrons with two different spin projections are different at a given distance from the localization potential. This difference can be considered to be produced by an effective magnetic field. Near the center of localization, the electron has spin projection $s = 1/2$ on the selected axis. At nonzero distance R from the donor, the spin projection on the same axis changes by an angle [2,5]:

$$\theta = \frac{2\alpha_{SO}\hbar}{\sqrt{2m_e E_g}}k_z^2 R = 0.0023\frac{R}{a_B}.$$ (11)

k_z^2 is the squared z component of the electron wave vector, with $k_z = \pi/L_z$ and $L_z = 16$ nm is the QW width. The value $\theta(R/a_B)$ is given here in radians. For clarity, we write the previous expression in degree units: $\theta(R/a_B) = 0.13R/a_B$. Therefore, to get the feeling of the order of rotation, to turn the spin by 1°, it is necessary to move away from the donor center by about $8a_B$. For comparison, for the dependence of θ on the distance from a donor in GaAs, $\theta = 1$ for $R = 10a_B$ [39,40].

The exchange constant for a pair of donors inside an infinite QW of thickness L_z is described by the following equation [5]:

$$2J(\hat{R}) = 2J_0 E_h^*[1 + (A\hat{R})^2]^{\beta/2}\exp[-\eta\hat{R} - \beta A\hat{R}\,\text{arctg}(A\hat{R})],$$ (12)

with $\hat{R} = R/a_B$. $a_B = 4.825$ nm is the Bohr radius [12]. $E_h^* = 51$ meV [41] is the Hartree energy [5]. $2J_0 = 1$, $A = 0.6$, $\beta = 2$, and $\eta = 0.1$ are the parameters extracted from Ref. [41]. Hence, $J(\hat{R}) = 132$ μeV for the presented parameters.

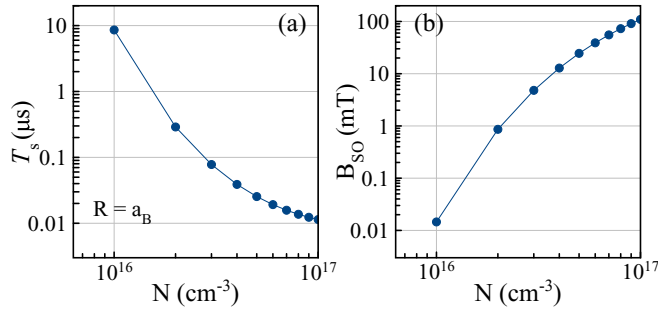Since the electrons are located at different distances from the donors, any selected electron experiences a random

FIG. 11. The dependence of T_s (a) and B_{SO} (b) on the donor concentration N for 16 nm QW. Here $\alpha = 1$.

fluctuating effective magnetic field by the surrounding electron spins. The exchange interaction in an ensemble of randomly oriented electron spins leads to an acceleration of the spin relaxation. The spin-relaxation time can be determined as follows [2,5]:

$$T_s = \frac{L_{SO}^2}{2\zeta D_{ex}}, \tag{13}$$

$L_{SO} = R/\theta = 2.1 \ \mu$m is the spin-orbit length. $\zeta = 0.8$ is the numerical factor of the order of one [5]. $3D_{ex} = r^2 J/\hbar$ is the spin diffusion coefficient, J is the exchange constant averaged over an infinite donor cluster with different distances between the donors, and r is the average distance between donors. Using

$$r = 0.5\alpha N_{2D}^{-1/2}, \tag{14}$$

$N_{2D} = NL_z$ is the concentration of donors per cm^{-2}. α is a coefficient ranging between 1 and 2 ($\alpha = 1.73$ for GaAs). For example, for a concentration of $N = 3 \times 10^{16}$ cm^{-3} and $\alpha = 1$, the average distance between donors is $r = 23$ nm.

The spin-diffusion coefficient can be estimated as [2]

$$D_{ex} = \frac{Jr^2}{3\hbar} = 0.35 \ \text{cm}^2/\text{s}. \tag{15}$$

As a result, the spin-relaxation time for the concentration $N = 3 \times 10^{16}$ cm^{-3} and $\alpha = 1$ is $T_s = 78$ ns. The actual concentration of fluorine atoms may differ from background carrier concentration due to the presence of fluorine atoms in the MBE chamber. Additionally, the estimated spin-relaxation time is higher than experimentally observed ($T_s = 30$ ns) due to measuring at a nonzero pump power. As noted earlier, we are not able to estimate T_s with zero pump power due to carrier-type dependence on the pump power. Therefore, we can assume that it is higher than 30 ns [15].

The value of the effective magnetic field can be estimated from the exchange constant and the spin rotation angle of the electron spin [Eq. (17) in Ref. [2]]:

$$\hbar\Omega_{SO} = \theta J, \tag{16}$$

$$B_{SO} = \frac{\hbar\Omega_{SO}}{\mu_B g_e}. \tag{17}$$

As an example, for $R = a_B$ the $\theta = 0.0023$ and $B_{SO} = 4.8$ mT. This value is close to the $B_{1/2} = 1.5$ mT given in Fig. 10(b). Figure 11 shows the dependence of T_s and B_{SO} on

the donor concentration N. An increase in donor concentration leads to a faster spin relaxation, as the value of the effective magnetic field increases.

Let us consider now the mechanism of exchange interaction for heavy holes [42]. The rotation angle of the spin of a heavy hole at some distance from the acceptor is given by [42]

$$\theta_h = \frac{4\sqrt{3}m_h \varkappa}{\hbar^2} R_h, \tag{18}$$

$\varkappa \approx 10^{-10}$ eV cm is constant for a linear wave-vector term taking into account the spin-orbit mixing of the Γ_{15v} and Γ_{12} zones. The constants for different semiconductors are given in Ref. [43]. Since $\varkappa$ is in the same order for different semiconductors, one can use the above value for ZnSe to obtain a rough estimate. So, for a heavy hole, the angle of rotation on distance R_h from an acceptor is $\theta_h = 0.11R_h/a_B$. Therefore, the spin of the hole turns by $6°$ at a distance of one Bohr radius from the acceptor.

The Bohr radius for heavy holes localized on impurity centers is calculated using the following equation:

$$a_{B,h} = 1.5\epsilon a_{hd} m_0/m_h, \tag{19}$$

where $\epsilon = 8.8$ is the dielectric constant for ZnSe, $a_{hd} = 0.053$ nm is the Bohr radius of the hydrogen atom, m_0 is the electron mass, and $m_h = 0.96m_0$ is the effective mass of the heavy hole. This gives us for the Bohr radius $a_{B,h} = 1.1$ nm. Hence, the exchange constant (J_h) for localized holes is extremely small due to its exponential dependence on the Bohr radius. The relaxation time of heavy holes in our experiments is in the same order as for the electrons. Therefore, based on these estimations, we can conclude that the spin-orbit mechanism is not responsible for the spin relaxation of the holes localized on acceptors. On the other hand, based on the observations, we can also argue that the majority of heavy holes is not localized on acceptors (if present at all), but rather on the potential fluctuations.

Finally, these conclusions allow us to relate the observed PRC widths in Fig. 10 to the effective magnetic field caused by the spin-orbit exchange interaction.

V. CONCLUSIONS

We have presented results for the spin dynamics of electrons and holes in an isotopically purified ZnSe/(Zn,Mg)Se quantum well under various excitation conditions. The spin dephasing times, the g-factor values, their spreads, and anisotropies of g factors have been measured for electrons and holes. For holes, this time is quite long (up to 19 ns). The presence of only one zero-field peak in the RSA signal, measured in the spectral region of the positive trion, is explained by the significant dispersion of the hole g factor (up to 67%). The possibility of switching of the structure from p type to n type has been demonstrated by additional above-barrier illumination or by an increase of the excitation intensity. We suggest that the electron and hole spin-relaxation time in this isotopically purified material is determined by the spin-orbit exchange interaction, whereby the electrons are preferentially localized at fluorine donors, while the holes populate the potential minima caused by fluctuating QW thickness.

[1] *Spin physics in semiconductors*, edited by M. I. Dyakonov (Springer-Verlag, Berlin 2008).

[2] K. V. Kavokin, Spin relaxation of localized electrons in n-type semiconductors, Semicond. Sci. Technol. **23**, 114009 (2008).

[3] R. I. Dzhioev, V. L. Korenev, B. P. Zakharchenya, D. Gammon, A. S. Bracker, J. G. Tischler, and D. S. Katzer, Optical orientation and the Hanle effect of neutral and negatively charged excitons in GaAs/Al_xGa_{1-x}As quantum wells, Phys. Rev. B **66**, 153409 (2002).

[4] T. Korn, Time-resolved studies of electron and hole spin dynamics in modulation-doped GaAs/AlGaAs quantum wells, Phys. Rep. **494**, 415 (2010).

[5] G. Garcia-Arellano, F. Bernardot, G. Karczewski, C. Testelin, and M. Chamarro, Spin relaxation time of donor-bound electrons in a CdTe quantum well, Phys. Rev. B **99**, 235301 (2019).

[6] E. A. Zhukov, D. R. Yakovlev, M. Gerbracht, G. V. Mikhailov, G. Karczewski, T. Wojtowicz, J. Kossut, and M. Bayer, Spin coherence of holes and electrons in undoped CdTe/(Cd, Mg)Te quantum wells, Phys. Rev. B **79**, 155318 (2009).

[7] E. A. Zhukov, D. R. Yakovlev, M. Bayer M. M. Glazov, E. L. Ivchenko, G. Karczewski, T. Wojtowicz, and J. Kossut, Spin coherence of a two-dimensional electron gas induced by resonant excitation of trions and excitons in CdTe/(Cd, Mg)Te quantum wells, Phys. Rev. B **76**, 205310 (2007).

[8] E. A. Zhukov, A. Greilich, D. R. Yakovlev, K. V. Kavokin, I. A. Yugova, O. A. Yugov, D. Suter, G. Karczewski, T. Wojtowicz, J. Kossut, V. V. Petrov, Yu. K. Dolgikh, A. Pawlis, and M. Bayer, All-optical NMR in semiconductors provided by resonant cooling of nuclear spins interacting with electrons in the resonant spin amplification regime, Phys. Rev. B **90**, 085311 (2014).

[9] E. A. Zhukov, D. R. Yakovlev, A. Schwan, O. A. Yugov, A. Waag, L. W. Molenkamp, and M. Bayer, Spin coherence of electrons and holes in ZnSe-based quantum wells studied by pump-probe Kerr rotation, Phys. Status Solidi B **251**, 1872 (2014).

[10] E. A. Chekhovich, A. Ulhaq, E. Zallo, F. Ding, O. G. Schmidt, and M. S. Skolnick, Measurement of the spin temperature of optically cooled nuclei and GaAs hyperfine constants in GaAs/AlGaAs quantum dots, Nat. Mater. **16**, 982 (2017).

[11] A. Pawlis, G. Mussler, C. Krause, B. Bennemann, U. Breuer, and D. Grützmacher, MBE growth and optical properties of isotopically purified ZnSe heterostructures, ACS Appl. Electron. Mater. **1**, 44 (2019).

[12] A. Greilich, A. Pawlis, F. Liu, O. A. Yugov, D. R. Yakovlev, K. Lischka, Y. Yamamoto, and M. Bayer, Spin dephasing of fluorine-bound electrons in ZnSe, Phys. Rev. B **85**, 121303 (2012).

[13] *Semiconductor spintronics and quantum computation*, edited by D. D. Awschalom, D. Loss, and N. Samarth (Springer-Verlag, Berlin, 2002).

[14] J. M. Kikkawa and D. D. Awschalom, Resonant Spin Amplification in n-Type GaAs, Phys. Rev. Lett. **80**, 4313 (1998).

[15] F. Heisterkamp, E. A. Zhukov, A. Greilich, D. R. Yakovlev, V. L. Korenev, A. Pawlis, and M. Bayer, Longitudinal and transverse spin dynamics of donor-bound electrons in fluorine-doped ZnSe: Spin inertia versus Hanle effect, Phys. Rev. B **91**, 235432 (2015).

[16] D. S. Smirnov, E. A. Zhukov, E. Kirstein, D. R. Yakovlev, D. Reuter, A. D. Wieck, M. Bayer, A. Greilich, and M. M. Glazov, Theory of spin inertia in singly charged quantum dots, Phys. Rev. B **98**, 125306 (2018).

[17] E. A. Zhukov, E. Kirstein, D. S. Smirnov, D. R. Yakovlev, M. M. Glazov, D. Reuter, A. D. Wieck, M. Bayer, and A. Greilich, Spin inertia of resident and photoexcited carriers in singly charged quantum dots, Phys. Rev. B **98**, 121304(R) (2018).

[18] I. A. Yugova, M. M. Glazov, D. R. Yakovlev, A. A. Sokolova, and M. Bayer, Coherent spin dynamics of electrons and holes in semiconductor quantum wells and quantum dots under periodical optical excitation: Resonant spin amplification versus spin mode locking, Phys. Rev. B **85**, 125304 (2012).

[19] S. Varwig, A. Schwan, D. Barmscheid, C. Müller, A. Greilich, I. A. Yugova, D. R. Yakovlev, D. Reuter, A. D. Wieck, and M. Bayer, Hole spin precession in a (In, Ga)As quantum dot ensemble: From resonant spin amplification to spin mode locking, Phys. Rev. B **86**, 075321 (2012).

[20] X. Marie, T. Amand, P. Le Jeune, M. Paillard, P. Renucci, L. E. Golub, V. D. Dymnikov, and E. L. Ivchenko, Hole spin quantum beats in quantum-well structures, Phys. Rev. B **60**, 5811 (1999).

[21] G. V. Astakhov, D. R. Yakovlev, V. P. Kochereshko, W. Ossau, W. Faschinger, J. Puls, F. Henneberger, D. Wolverson, N. A. Gippius, and A. Waag, Binding energy of charged excitons in ZnSe-based quantum wells, Phys. Rev. B **65**, 165335 (2002).

[22] J. L. Merz, H. Kukimoto, K. Nassau, and J. W. Shiever, Optical properties of substitutional donors in ZnSe, Phys. Rev. B **6**, 545 (1972).

[23] A. Pawlis, T. Berstermann, C. Brüggemann, M. Bombeck, D. Dunker, D. R. Yakovlev, N. A. Gippius, K. Lischka, and M. Bayer, Exciton states in shallow ZnSe/(Zn, Mg)Se quantum wells: Interaction of confined and continuum electron and hole states, Phys. Rev. B **83**, 115302 (2011).

[24] I. A. Yugova, M. M. Glazov, E. L. Ivchenko, and Al. L. Efros, Pump-probe Faraday rotation and ellipticity in an ensemble of singly charged quantum dots, Phys. Rev. B **80**, 104436 (2009).

[25] M. M. Glazov and E. L. Ivchenko, Resonant spin amplification in nanostructures with anisotropic spin relaxation and spread of the electronic *g* factor, Fiz. Techn. Polupr. **42**, 966 (2008) [Semiconductors **42**, 951 (2008)].

[26] A. V. Khaetskii, D. Loss, and L. Glazman, Electron Spin Decoherence in Quantum Dots Due to Interaction with Nuclei, Phys. Rev. Lett. **88**, 186802 (2002).

[27] E. A. Chekhovich, M. M. Glazov, A. B. Krysa, M. Hopkinson, P. Senellart, A. Lemaître, M. S. Skolnick, and A. I. Tartakovskii, Element-sensitive measurement of the hole-nuclear spin interaction in quantum dots, Nat. Phys. **9**, 74 (2013).

[28] B. Eble, C. Testelin, P. Desfonds, F. Bernardot, A. Balocchi, T. Amand, A. Miard, A. Lemaitre, X. Marie, and M. Chamarro, Hole-Nuclear Spin Interaction in Quantum Dots, Phys. Rev. Lett. **102**, 146601 (2009).

[29] P. Fallahi, S. T. Yilmaz, and A. Imamoğlu, Measurement of a Heavy-Hole Hyperfine Interaction in InGaAs Quantum Dots Using Resonance Fluorescence, Phys. Rev. Lett. **105**, 257402 (2010).

[30] M. Y. Petrov, I. V. Ignatiev, S. V. Poltavtsev, A. Greilich, A. Bauschulte, D. R. Yakovlev, and M. Bayer, Effect of thermal annealing on the hyperfine interaction in InAs/GaAs quantum dots, Phys. Rev. B **78**, 045315 (2008).

[31] I. A. Merkulov, Al. L. Efros, and M. Rosen, Electron spin relaxation by nuclei in semiconductor quantum dots, Phys. Rev. B **65**, 205309 (2002).

[32] *Optical orientation*, edited by F. Meier and B. P. Zakharchenya (North-Holland, Amsterdam, 1984).

[33] F. Heisterkamp, A. Greilich, E. A. Zhukov, E. Kirstein, T. Kazimierczuk, V. L. Korenev, I. A. Yugova, D. R. Yakovlev, A. Pawlis, and M. Bayer, Inhomogeneous nuclear spin polarization induced by helicity-modulated optical excitation of fluorine-bound electron spins in ZnSe, Phys. Rev. B **92**, 245441 (2015).

[34] F. Heisterkamp, E. Kirstein, A. Greilich, E. A. Zhukov, T. Kazimierczuk, D. R. Yakovlev, A. Pawlis, and M. Bayer, Dynamics of nuclear spin polarization induced and detected by coherently precessing electron spins in fluorine-doped ZnSe, Phys. Rev. B **93**, 081409(R) (2016).

[35] E. A. Zhukov, E. Kirstein, N. E. Kopteva, F. Heisterkamp, I. A. Yugova, V. L. Korenev, D. R. Yakovlev, A. Pawlis, M. Bayer, and A. Greilich, Discretization of the total magnetic field by the nuclear spin bath in fluorine-doped ZnSe, Nat. Commun. **9**, 1941 (2018).

[36] A. Abragam, *The principle of nuclear magnetism* (Oxford University Press, Oxford, 1961).

[37] L. D. Landau and E. M. Lifshitz, *Quantum mechanics. Nonrelativistic theory* (Pergamon, Oxford, 1965).

[38] M. Cardona, N. E. Christensen, and G. Fasol, Relativistic band structure and spin-orbit splitting of zinc-blende-type semiconductors, Phys. Rev. B **38**, 1806 (1988).

[39] L. P. Gor'kov, and P. L. Krotkov, Spin relaxation and antisymmetric exchange in n-doped III-V semiconductors, Phys. Rev. B **67**, 033203 (2003).

[40] K. V. Kavokin, Anisotropic exchange interaction of localized conduction-band electrons in semiconductors, Phys. Rev. B **64**, 075305 (2001).

[41] G. Garcia-Arellano, F. Bernardot, C. Testelin and M. Chamarro, Electron exchange energy of neutral donors inside a quantum well, Phys. Rev. B **98**, 195308 (2018).

[42] K. V. Kavokin, Symmetry of anisotropic exchange interactions in semiconductor nanostructures, Phys. Rev. B **69**, 075302 (2004).

[43] G. E. Pikus, V. A. Marushchak, and A. N. Titkov, Spin splitting and carrier spin relaxation in cubic crystals $A_{III}B_V$, Fiz. Tekh. Poluprovodn. **22**, 185 (1988) [Sov. Phys. Semicond. **22**, 115 (1988)].